Electronic asymmetry in self-assembled quantum dot molecules made of identical InAs/GaAs quantum dots

Lixin He, Gabriel Bester, and Alex Zunger

National Renewable Energy Laboratory, Golden, Colorado 80401, USA

We show that a diatomic dot molecule made of two identical, vertically stacked, strained InAs/GaAs self-assembled dots exhibits an asymmetry in its single- and many-particle wave functions. The single particle wave function is asymmetric due to the inhomogeneous strain, while the asymmetry of the many-particle wave functions is caused by the correlation-induced localization: the lowest singlet $^1\Sigma_g$ and triplet $^3\Sigma$ states show that the two electrons are each localized on different dots within the molecule; for the next singlet states $^1\Sigma_u$ both electrons are localized on the same (bottom) dot for interdot separation $d > 8$ nm. The singlet-triplet splitting is found to be ~0.1 meV at interdot separation $d=9$ nm and as large as 100 meV for $d=4$ nm, orders of magnitude larger than the few meV found in the large (50–100 nm) electrostatically confined dots.

Quantum dot molecules (QDM) occupied by two electronic spins have been proposed as a basis for quantum computation.[1] Loss and DiVincenzo[2] proposed a "swap gate" based on a simplified model in which the two localized spins have Heisenberg coupling $H = J_{S\text{-}T}\vec{S}_1 \cdot \vec{S}_2$, where $\vec{S}_1$ and $\vec{S}_2$ are the spin-$\frac{1}{2}$ operators for the two localized electrons and $J_{S\text{-}T}$ is the effective Heisenberg exchange splitting, being the difference in energy between the spin-triplet state with total spin $S=1$ and the spin-singlet state with $S=0$. Successful operation would require a large singlet-triplet splitting $J_{S\text{-}T}$ (fast swap time[2]) and that the probability $Q_{\text{tot}}^{(\nu)}$ of the two electrons in state ν simultaneously occupying one dot be small (maximizing entanglement[3]). The search for a nanosystem with large $J_{S\text{-}T}$ and small $Q_{\text{tot}}^{(\nu)}$ involves engineering of the properties of the corresponding many-particle wave functions. In a simplified molecular model, the single-particle wave functions of the two electrons are given by bonding $\psi_{\sigma_g} = (\chi_T + \chi_B)/\sqrt{2}$ and antibonding $\psi_{\sigma_u} = (\chi_T - \chi_B)/\sqrt{2}$ molecular orbitals, constructed from the individual orbitals χ of the top (T) and bottom (B) dot. The many-particle states are then the corresponding product states $|\sigma_g^\uparrow \sigma_g^\downarrow\rangle \sim {}^1\Sigma_g$ (singlet), $|\sigma_g^\uparrow \sigma_u^\uparrow\rangle \sim {}^3\Sigma$ (triplet), etc. In this picture both single-particle molecular orbitals and the many-particle states are delocalized on both dots constituting the dot molecule. Here, we discuss via atomistic single-particle and many-body calculations two important deviations from this simplified molecular picture, leading to asymmetries both in the single-particle molecular orbitals due to the inhomogeneous strains, and in the many-body states (i.e., localization either on T or on B) as a consequence of correlation. For the many-body states we find Mott-like transitions for the first and third singlet states: both electrons are localized on one dot at large d and delocalized over both dots at small d. The double occupancy $Q_{\text{tot}}^{(\nu)}$ of the first singlet state is surprisingly large ($\simeq 40\%$) for an interdot separation of 5 nm. The triplet states and the second singlet state are Mott localized at every interdot separations with $Q_{\text{tot}}^{(\nu)} = 0$ (no double occupation) for the triplet states and $Q_{\text{tot}}^{(\nu)} = 1$ for the singlet state.

Previous models of dot molecules have focused on electrostatically confined dots,[4–6] which have a very large confining dimension of 50–100 nm. Such dots exhibit typical single-particle level spacings of $\Delta\epsilon_e = 3$–5 meV, Coulomb energies J_{ee} of about 5 meV $\gtrsim \Delta\epsilon_e$, whereas exchange energies and correlation energies are around 1 meV. Many experiments were recently done on *two* such coupled dots,[7,8] showing that the splitting between the bonding and antibonding molecular levels is as large as 3.5 meV at an interdot separation of 2.5 nm, comparable to the single-particle energy spacing $\Delta\epsilon_e$ of the single dot. Because of the very large size of such dots, their single-particle levels can be described by simple one-band effective-mass "particle-in-a-box" models using the external potential generated by a combination of band offset, the gate potential, and the ionized impurities.[9,10] Alternatively, one can simply assume a particle-in-a-parabolic well model.[11,12] In these descriptions, the single-particle states are symmetric, but many-electron symmetry breaking is possible due to correlation effects, as shown via unrestricted Hartree-Fock treatment of the effective-mass approximation (UHF-EMA) (Ref. 13), configuration-interaction treatment of the effective-mass approximation (CI-EMA) (Ref. 12), or Mott-Hubbard model.[14]

Here, we discuss localization effects and singlet-triplet splitting of electrons in vertically coupled self-assembled InAs/GaAs quantum dot molecules grown epitaxially.[15–17] Such dots have much smaller confining dimensions (height of 3–5 nm), and when made of InAs/GaAs their electronic level splitting is $\Delta\epsilon_e \sim 40$–50 meV, *larger* than the interelectronic Coulomb repulsion $J_{ee} \sim 10$–20 meV, and the exchange energy $K_{ee} \sim 2$–5 meV. In this paper, we show that in vertically aligned self-assembled dots, one can achieve singlet-triplet splittings of up to 100 meV.

Figure 1(a) shows the geometry selected for the dot molecules, consisting of two-dimensional InAs wetting layers, a pair of 2-nm-tall InAs dots in the shape of truncated cones embedded in a GaAs matrix. The considered dots are identical and describe the experimental extreme case of perfect growth. In reality, both dots can be geometrically and compositionally different. This extrinsic inequivalence would reinforce the intrinsic asymmetry of the system which our results describe. The hydrostatic strain field $\text{Tr}(\epsilon)$, with the isostrain lines shown in Fig. 1(a), is calculated atomistically by relaxing the bond-stretching and bond-bending forces ac-
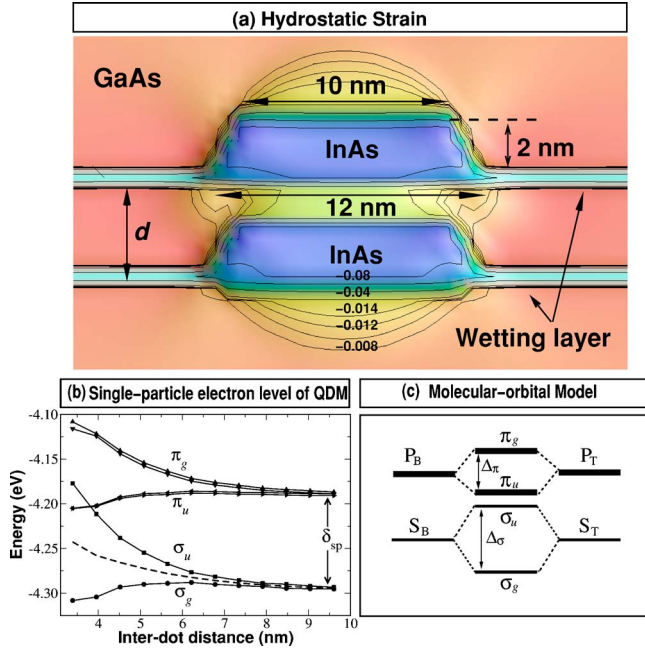
FIG. 1. (Color online) (a) Contour plot of the hydrostatic strain Tr(ϵ) in the two vertically coupled quantum dots. The interdot distance d is measured from one wetting layer to the next. The iso-strain values are also marked in the figure. (b) Molecular-orbital energy levels vs interdot distance. The dashed line is the average of σ_g and σ_u. δ_{sp} is the single dot s-p energy-level splitting. (c) Sketch of bonding-antibonding splitting. S_T, S_B are "s" while P_T and P_B are "p" single dot orbitals on top and bottom dots. Here $S_T+S_B=\sigma_g$ and $P_T+P_B=\pi_u$ are bonding states, while the $S_T-S_B=\sigma_u$ and P_T-P_B $=\pi_g$ are antibonding states.

cording to the valence force-field model (VFF) (Refs. 18 and 19). It is clearly seen in Fig. 1(a) that both dots have large and nearly constant hydrostatic strain inside the dots which decays rapidly outside the dots. However, even though the dots comprising the molecule are the same, the strain on the two dots is different since the molecule lacks inversion symmetry. We see that the top dot is slightly more strained than the bottom dot. Furthermore, the GaAs region *between* the two dots is much more strained than in other parts of the matrix.

Having established a realistic geometry and the relaxed atomic positions $\{\mathbf{R}_{m,\alpha}\}$, we calculate the single-particle electronic structure by constructing a pseudopotential $V(\mathbf{r})$ $=\Sigma_{m,\alpha}v_\alpha(\mathbf{r}-\mathbf{R}_{m,\alpha})$ from a superposition of screened atomic potentials v_α of species $\alpha=$ Ga, In, As. Here, v_α is constructed[20] by fitting to available experimental data the bulk InAs and GaAs band energies, effective masses, hydrostatic and biaxial deformation potentials, and band offsets. The pseudopotentials used in present work are taken from Ref. 20. The Schrödinger equation is solved by the linear combination of bulk bands (LCBB) (Ref. 21), method in a Bloch orbitals basis $\{\phi_{n,\mathbf{k},\vec{\epsilon}}^{(\lambda)}(\mathbf{r})\}$ of band index n and wave vector $\mathbf{k}$ of material λ (=InAs, GaAs). The basis functions are strained uniformly to constant but different strains $\vec{\epsilon}$. We use $\vec{\epsilon}=0$ for the (unstrained) GaAs matrix material, and an average $\vec{\epsilon}$ value from VFF for the strained dot material

(InAs). For the InAs/GaAs system, we use $n=2$ for electron states on a $6\times6\times28$ k mesh. Unlike the effective-mass description of single-particle state used for electrostatic dot,[9–12] here we allow interband and intervalley coupling.

Asymmetry of single-particle states. Figure 1(b) shows the single-particle dot-molecule energy levels as a function of interdot distance d. These results can be generally understood using bonding and antibonding molecular orbitals as shown in Fig. 1(c). At large d, the energy levels converge to those of single dots, showing an s level and, at δ_{sp} $=106$ meV higher, two p levels split by a few meV reflecting the atomistic C_{2v} symmetry of the cylindrically symmetric dots.[22] Bonding and antibonding molecular orbitals form when the two dots interact: the two single-dot s orbitals form molecular σ_g and σ_u orbitals, whereas the four single-dot p orbitals (two on each dot) form two molecular π_u and two molecular π_g orbitals.[12] Note that the splitting of σ_g from σ_u is not symmetric, as can be seen by looking at the average of both energies in Fig. 1(b) (dashed line). The average energy increases with decreasing interdot separation in response to the strain exerted by the presence of the other dot [Fig. 1(a)]. Beyond this overall effect, the strain field is different on both geometrically identical dots because the dots are nonspherical [Fig. 1(a)] and lack inversion symmetry. This causes an asymmetry of the molecular orbitals at short interdot distances. At $d\sim3.4$ nm, we found that the bonding (antibonding) states are slightly more localized on the bottom (top) dot. In previous effective-mass calculations,[7,8,11–13] strain effects were not included and single-particle asymmetry was not found. Particularly, in Ref. 7, an *ad hoc* parameter was introduced to force the asymmetry of the dot molecule.

A more quantitative analysis of the asymmetry can be given when the molecular orbitals are transformed via a Wannier-like transformation into single dot states. These can be obtained from a unitary rotation of *molecular* orbitals ψ_i,

$$\chi_{l,p} = \sum_i \mathcal{U}_{l,p}^{(i)}\psi_i, \tag{1}$$

where ψ_i is the ith molecular orbital and $\chi_{l,p}$ are the rotated, dot-centered orbitals (the lth orbital localized on $p=T$ or B dot). $\mathcal{U}$ are unitary matrices, $\mathcal{U}^\dagger\mathcal{U}=I$, chosen to maximize the total self-Coulomb energy.[23,24] Once $\mathcal{U}_{l,p}^{(i)}$ are known, we define the orbital energies of the dot-centered states $\chi_{l,p}$ as

$$e_{l,p} = \langle\chi_{l,p}|\hat{T}|\chi_{l,p}\rangle = \sum_i (\mathcal{U}_{l,p}^{(i)})^*\mathcal{U}_{l,p}^{(i)}\epsilon_i, \tag{2}$$

where $\hat{T}$ is the kinetic-energy operator and ϵ_i is the energy of the ith molecular orbital. The energies $e_{l,p}$ of the dot-centered orbitals are depicted in Fig. 2(a) as a function of the interdot separation. We see that the single-particle energies for both B and T orbitals rise quickly as the interdot distance is reduced, but the energy of the top dot orbital raises faster. At $d\sim3.4$ nm, there is an energy splitting of ~12 meV between top and bottom dot orbitals, which causes the asymmetry of the wave functions between top and bottom dots.

Many-particle symmetry breaking. Having obtained the "molecular," single-particle energy [Fig. 1(b)], and wave functions, we calculate all interelectronic Coulomb and exchange integrals J and K of ψ_i by numerical integration,[25] and set up a screened configuration-interaction expansion.[26]
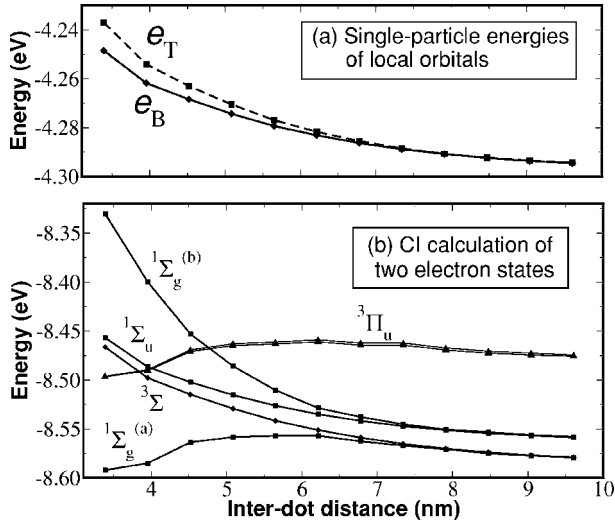
FIG. 2. (a) The effective single-particle energy levels e_T and e_B of dot-centered orbitals on the top dot and bottom dot, respectively. (b) Energy of two-electron states calculated from CI using all confined molecular orbitals.

A microscopic position-dependent dielectric screening[26] is applied to both Coulomb and exchange integrals to represent the inner electrons that are not calculated explicitly. Considering six molecular orbitals $\sigma_g, \sigma_u, \pi_u, \pi_g$ of Fig. 1(b), we have a total of 66 Slater determinants. The many-body wave functions Ψ_ν are written as linear combinations of these determinants $|\Phi_C\rangle$ as $\Psi_\nu = \Sigma_C A_\nu(C)|\Phi_C\rangle$. The resulting many-particle energies are shown as a function of interdot separation in Fig. 2(b). The energy splittings J_{S-T} between the ground-state singlet $^1\Sigma_g^{(a)}$ and triplet $^3\Sigma$ range from 0–100 meV and are much larger than in electrostatic dot molecules ($<$1 meV) (Refs. 4–6). In Fig. 3(a) we decompose the two-electron wave functions into the leading configurations $\Phi_1 = |\sigma_g^\uparrow \sigma_u^\downarrow\rangle$, $\Phi_2 = |\sigma_g^\downarrow \sigma_u^\uparrow\rangle$, $\Phi_3 = |\sigma_g^\uparrow \sigma_g^\downarrow\rangle$, and $\Phi_4 = |\sigma_u^\uparrow \sigma_u^\downarrow\rangle$. The ground state is the singlet $^1\Sigma_g^{(a)}$ state, followed by the threefold degenerated triplet states $^3\Sigma$ (we depict only the $s_z = 0$ state made of $\Phi_1 + \Phi_2$ in Fig. 3) and the next singlets $^1\Sigma_u$ (made of $\Phi_1 - \Phi_2$) and $^1\Sigma_g^{(b)}$.

To explore the symmetry breaking of these states, we plot in Figs. 3(b) and 3(c), the pair-correlation functions $P_\nu(\mathbf{r}_0, \mathbf{r}) = |\Psi_\nu(\mathbf{r}_0, \mathbf{r})|^2$ where $\mathbf{r}_0$ is fixed at the center of the bottom dot. $P_\nu(\mathbf{r}_0, \mathbf{r})$ gives the probability of finding the second electron at position $\mathbf{r}$ given that the first electron has been found at $\mathbf{r}_0$. For the ground-state singlet $^1\Sigma_g^{(a)}$, we see that at the small interdot separation $d=4$ nm, the probability to find the second electron in the top or the bottom dot are comparable, suggesting a molecularlike delocalized state. Accordingly, the wave-function analysis reveals a dominant contribution from the product of two delocalized molecular orbitals Φ_3. By delocalizing into both dots, the electrons can lower their single-particle energy by about 65 meV (about half of the bonding-antibonding splitting), which overcome the Coulomb repulsion between the two electrons. With increasing interdot separation, the electrons show correlation-induced (i.e., the coupling between Φ_3 and Φ_4) localization. At $d=7$ nm, the second electron is almost entirely localized on the top dot as shown in Fig. 3(c). We emphasize that the many-particle wave-function localization is not due to the asymmetry in their single-particle wave functions. This is evident from the fact that in the absence of electron-electron correlations (no CI, see Ref. 24), the wave function is delocalized on *both* dots at all interdot distances. In contrast, once CI is introduced, the many-particle wave function is localized on one dot above a certain interdot separation, showing symmetry breaking. A similar delocalized-to-localized transition applies for the $^1\Sigma_g^{(b)}$ state, with the difference, that at large d both electrons are localized on the same (bottom) dot. In contrast, the triplet states $^3\Sigma$ and the singlet $^1\Sigma_u$ show localization at all interdot distances. However, for the triplet states the two electrons are localized on different dots while for $^1\Sigma_u$ both electrons are localized on the same dot.

To study the degree of localization quantitatively, we resort to the Wannier-like transformation of Eq. (1). The CI matrix elements expressed initially in the molecular basis ψ_i [Eq. (1)] are transformed into the dot-centered Wannier basis $\chi_{l,p}$ [Eq. (1)]. For example, $\{|\chi_{l,p}^\sigma, \chi_{l',p'}^{\sigma'}\rangle\}$ denotes the configuration where one electron is on the lth orbital of the p dot
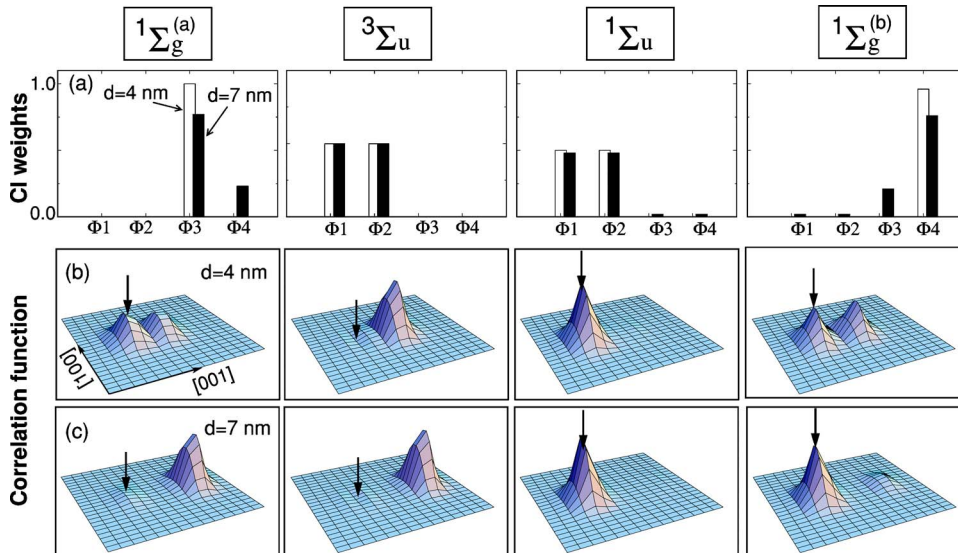

FIG. 3. (Color online) Panel (a) gives the weights of configurations Φ_1, Φ_2, Φ_3, and Φ_4 of the many-particle CI wave functions. Panels (b) and (c) depict the probability of finding the second electron at position $\mathbf{r}$ given that the first electron has been found on the center of the bottom dot (indicated by the arrows) for the interdot distances (b) $d=4$ nm and (c) $d=7$ nm.

with spin σ, and the other electron is on the l'th orbital of the p' dot with spin σ'. The two electrons can be either both on the top dots, or both on the bottom dots, or one on the top and the other on the bottom dots. We can thus define a "bielectron localization parameter" $Q_{pp}^{(\nu)}$ as the probability of two electrons occupying the dot $p=(T$ or $B)$ at the same time in the many-particle state ν,

$$Q_{pp}^{(\nu)} = \sum_{l\sigma,l'\sigma'} P_\nu (|\chi_{l,p}^\sigma, \chi_{l',p}^{\sigma'}\rangle), \qquad (3)$$

where $P_\nu(\mathcal{C})$ is the weight of the configuration $\mathcal{C}$ in the many-body wave functions of state ν. The total probability of two electrons being on the *same* dot is then $Q_{\text{tot}}^{(\nu)}=Q_{TT}^{(\nu)}+Q_{BB}^{(\nu)}$ for the νth state. Figure 4 shows the bielectron localization parameter $Q_{pp}^{(\nu)}$ of Eq. (3) for the many-particle states $\nu = {}^1\Sigma_g, {}^1\Sigma_u$. We see that: (i) the ground state ${}^1\Sigma_g^{(a)}$ has a very small Q_{pp} at large interdot separation ($d>8$ nm), whereas for the excited state ${}^1\Sigma_g^{(b)}$, the probability of two electrons being on the same dot is close to 1. For smaller d, Q_{tot} increases rapidly for ${}^1\Sigma_g^{(a)}$, while it decreases for ${}^1\Sigma_g^{(b)}$. At $d=4$ nm, $Q_{\text{tot}}({}^1\Sigma_g^{(a)}) \sim 0.5$, as a result of the fact that for the ground state, two electrons are delocalized into two dots, shown in Fig. 3(b). (ii) Our calculations show that the coupling between ${}^3\Sigma$ and higher triplet configurations is negligible, thus the calculated $Q_{pp}({}^3\Sigma)$ are zero (not shown), i.e., the electrons are on different dots, due to the Pauli principle. (iii) $Q_{\text{tot}}({}^1\Sigma_u)$ is close to 1 for all interdot distances [Fig. 4(b)] and both electrons are therefore occupying the same dots. As noted in the introduction, double occupation may lead to error in quantum computing, therefore it requires that $Q_{\text{tot}}^{(\nu)} \ll 1$, i.e., the electrons should be localized on different dots for the device. The requirements for quantum computation are best met for the ground state ${}^1\Sigma_g^{(a)}$ at an interdot distance of $6-8$ nm, where we have significant J_{S-T}, and Q_{tot} is small.

To conclude, we investigated the asymmetry of both single- and many-particle wave functions in the quantum dot molecules made of two identical, vertically stacked, InAs/GaAs self-assembled quantum dots. For the single-particle states, an asymmetry is introduced by the inhomoge-
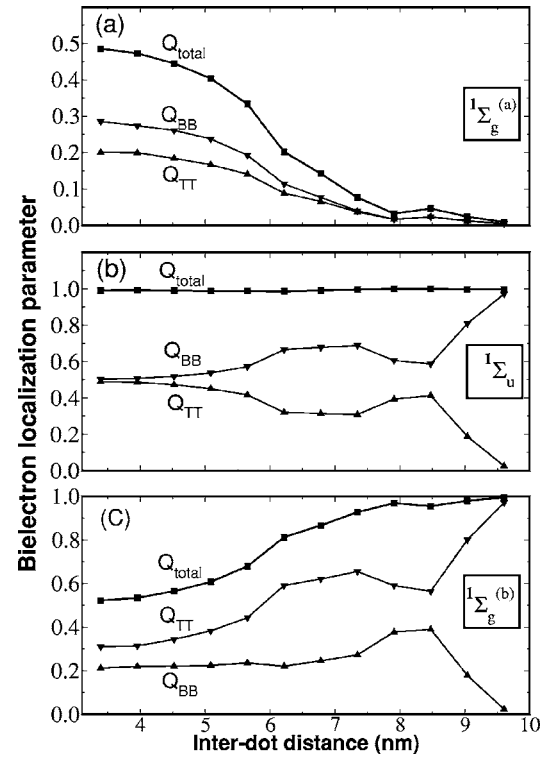

FIG. 4. The probability of two electrons occupying the same dot [Eq. (3)] for (a) ${}^1\Sigma_g^{(a)}$, (b) ${}^1\Sigma_u$, (c) ${}^1\Sigma_g^{(b)}$ states. Q_{TT} (Q_{BB}) is the probability of both electrons being on the top (bottom) dot, while Q_{total} gives the total probability.

neous strains, while for many-particle states, there is a symmetry breaking which can be characterized by wave-function localizations due to electron-electron correlations. We calculate the probability of "bielectron localization" as a function of interdot separations. We find that the ideal interdot separation where the two electron spins can be used for quantum information is around $6-8$ nm, where the singlet-triplet splitting is large but the double electron occupation still low.

[1] D. P. DiVincenzo, Science **270**, 255 (1995).
[2] D. Loss and D. P. DiVincenzo, Phys. Rev. A **57**, 120 (1998).
[3] J. Schliemann *et al.*, Phys. Rev. B **63**, 085311 (2001).
[4] R. C. Ashoori *et al.*, Phys. Rev. Lett. **68**, 3088 (1992).
[5] A. T. Johnson *et al.*, Phys. Rev. Lett. **69**, 1592 (1992).
[6] S. Tarucha *et al.*, Phys. Rev. Lett. **77**, 3613 (1996).
[7] M. Pi *et al.*, Phys. Rev. Lett. **87**, 066801 (2001).
[8] M. Rontani *et al.*, Phys. Rev. B **69**, 085327 (2004).
[9] L. R. C. Fonseca *et al.*, Phys. Rev. B **57**, 4017 (1998).
[10] S. Bednarek *et al.*, Phys. Rev. B **68**, 155333 (2003).
[11] X. Hu and S. DasSarma, Phys. Rev. A **61**, 062301 (2000).
[12] M. Rontani *et al.*, Solid State Commun. **119**, 309 (2001).
[13] C. Yannouleas *et al.*, Phys. Rev. Lett. **82**, 5325 (1999).
[14] C. A. Stafford *et al.*, Phys. Rev. Lett. **72**, 3590 (1994).

[15] D. Bimberg, M. Grundmann, and N. N. Ledentsov, *Quantum Dot Heterostructures* (Wiley, New York, 1999).
[16] T. Ota *et al.*, Superlattices Microstruct. **34**, 159 (2003).
[17] T. Ota *et al.*, Phys. Rev. Lett. **93**, 066801 (2004).
[18] P. N. Keating, Phys. Rev. **145**, 637 (1966).
[19] J. L. Martins and A. Zunger, Phys. Rev. B **30**, 6217 (1984).
[20] A. J. Williamson *et al.*, Phys. Rev. B **62**, 12963 (2000).
[21] L.-W. Wang and A. Zunger, Phys. Rev. B **59**, 15806 (1999).
[22] G. Bester and A. Zunger, Phys. Rev. B **71**, 045318 (2005).
[23] C. Edmiston *et al.*, Rev. Mod. Phys. **35**, 457 (1963).
[24] L. He, G. Bester, and A. Zunger, cond-mat/0503492 (unpublished).
[25] A. Franceschetti *et al.*, Phys. Rev. Lett. **78**, 915 (1997).
[26] A. Franceschetti *et al.*, Phys. Rev. B **60**, 1819 (1999).